Entanglement and entangling power of the dynamics in light-harvesting complexes

Filippo Caruso,[1,2,3,*] Alex W. Chin,[1,4] Animesh Datta,[2,3] Susana F. Huelga,[1,4] and Martin B. Plenio[1,2,3]
[1]*Universität Ulm, Institut für Theoretische Physik, Albert-Einstein-Allee 11, D-89069 Ulm, Germany*
[2]*QOLS, The Blackett Laboratory, Prince Consort Road, Imperial College, London, SW7 2BW, United Kingdom*
[3]*Institute for Mathematical Sciences, 53 Prince's Gate, Imperial College, London, SW7 2PG, United Kingdom*
[4]*School of Physics, Astronomy & Mathematics, University of Hertfordshire, Hatfield, AL10 9AB, United Kingdom*
(Received 11 December 2009; published 28 June 2010)

We study the evolution of quantum entanglement during exciton energy transfer (EET) in a network model of the Fenna-Matthews-Olson (FMO) complex, a biological pigment-protein complex involved in the early steps of photosynthesis in sulfur bacteria. The influence of Markovian as well as spatially and temporally correlated (non-Markovian) noise on the generation of entanglement across distinct chromophores (site entanglement) and different excitonic eigenstates (mode entanglement) is studied for different injection mechanisms, including thermal and coherent laser excitation. Additionally, we study the entangling power of the FMO complex under natural operating conditions. While quantum information processing tends to favor maximal entanglement, near unit EET is achieved as the result of an intricate interplay between coherent and noisy processes where the initial part of the evolution displays intermediate values of both forms of entanglement.

DOI: 10.1103/PhysRevA.81.062346 PACS number(s): 03.67.−a, 03.65.Ud, 03.65.Yz

I. INTRODUCTION

Photosynthesis, at its simplest, is the absorbtion of sunlight by photosensitive antennae and its subsequent conversion into chemical energy at a reaction center. The locations for these processes are physically and physiologically separated, which forces nature to devise a way to transfer the solar energy from the antennae to the reaction center (RC). Exciton energy transfer (EET) is facilitated by certain protein molecules called light-harvesting complexes, and occurs at efficiencies of about 99%. EET has been a subject of continual interest for decades, not only for its phenomenal efficiency but also for its fundamental role in nature [1]. Recently, ultrafast optics and nonlinear spectroscopy experiments have provided new insights into the process of EET in light-harvesting complexes, like the one found in purple bacteria (LH-I) and the Fenna-Matthew-Olson (FMO) complex [2,3]. In particular, evidence of quantum coherence has been presented, with the idea that nontrivial quantum effects may be at the root of its remarkable efficiency [4]. Following this, several studies have attempted to unravel the precise role of quantum coherence in the EET of light-harvesting complexes [5–11] and have, perhaps surprisingly, found that environmental decoherence and noise plays a crucial role [5–8,12].

Light-harvesting complexes consist of several chromophores mutually coupled by dipolar interactions residing within a protein scaffold. Due to their mutual coupling, light-induced excitations on individual chromophores (sites) can undergo coherent transfer from site to site, and the typical eigenstates are therefore delocalized over multiple chromophores. It is in these eigenstates, henceforth referred to as exciton states, that one finds evidence of quantum coherence. Here, we will study the role of quantum coherence in the process of EET in the FMO complex, as quantified by quantum entanglement, and investigate the sensitivity of the entanglement dynamics to variables that have not been directly measured, such as the microscopic interaction strength between the complex and the surrounding environment, and the possible existence of spatial and temporal correlations in the bath. In this context, the first analysis of the entanglement behavior in light-harvesting complexes was presented in Ref. [7], in which we analyzed the evolution of an entanglement measurement (i.e., logarithmic negativity [13,14]) in a Markovian model of the FMO complex. The scope of the present work is two fold; on the one hand it aims to make the study of coherence and entanglement in such systems quantitative by considering spatial and temporal (non-Markovian) noise correlations and, secondly, it uses this quantitative approach to show that maximal entanglement is not correlated with optimal transport, a result that may shed light on the possible functional role of entanglement in EET.

Entanglement is defined between subsystems of a global system. When considering entanglement in a composite system whose components are closely spaced and strongly interacting, as in the FMO complex, this choice of subsystems is, to some extent, dictated by the way we interrogate the system. If the sites can be addressed individually, then it is operationally well justified to speak about site-entanglement, i.e., quantum correlations across distinguishable locations. However, if we are limited to accessing the global excitations of the systems, i.e., the excitonic eigenstates of the Hamiltonian governing the dynamics of the FMO complex, then we will speak of mode entanglement as we then explore entanglement between the eigenmodes of the system (for more details on entanglement theory and its essential foundations see Ref. [14]). Here, we will explore both types of correlations but place a perhaps greater emphasis on the aspects of site entanglement, which is more closely linked to the nonlocal structure of quantum correlations. In general, the presence of quantum coherence, signified by the presence of off-diagonal elements in the density matrix, is necessary but not sufficient for the presence of quantum entanglement [14]. However, the two conditions are equivalent if one makes the idealized assumption that there is a single excitation in the system. In this work, as explained below, our entanglement analysis

*filippo.caruso@uni-ulm.de

also goes beyond the single-excitation approximation and takes into account different experimental and natural operating conditions for the FMO complex dynamics.

This article is organized as follows: In Sec. II we introduce the theoretical model for the FMO dynamics and discuss the entanglement measure used here. Then, we analyze the logarithmic negativity and the so-called entangling power in some non-Markovian FMO models in Sec. III and generalize these results for different injection schemes (i.e., thermal injection and laser excitation of the FMO complex) in Sec. IV. Finally, the entanglement between excitons (mode entanglement) is investigated in Sec. V and the conclusions and final remarks are presented in Sec. VI.

II. SITE ENTANGLEMENT

Each chromophore (site) in the FMO complex can be represented by a two-state system (qubit). As in Ref. [7], the effective dynamics is modelled by an $N = 7$ qubit Hamiltonian which describes the coherent exchange of excitations between sites, that is,

$$H = \sum_{j=1}^{7} \hbar\omega_j \sigma_j^+ \sigma_j^- + \sum_{j\neq l} \hbar v_{j,l} (\sigma_j^- \sigma_l^+ + \sigma_j^+ \sigma_l^-), \quad (1)$$

and local Lindblad terms that take into account the dissipation and dephasing caused by the surrounding environment, namely,

$$\mathcal{L}_{\text{diss}}(\rho) = \sum_{j=1}^{7} \Gamma_j [-\{\sigma_j^+ \sigma_j^-, \rho\} + 2\sigma_j^- \rho \sigma_j^+] \quad (2)$$

and

$$\mathcal{L}_{\text{deph}}(\rho) = \sum_{j=1}^{7} \gamma_j [-\{\sigma_j^+ \sigma_j^-, \rho\} + 2\sigma_j^+ \sigma_j^- \rho \sigma_j^+ \sigma_j^-]. \quad (3)$$

This Markovian form of the evolution preserves complete positivity, an essential feature when evaluating entanglement, as discussed below. Here σ_j^+ (σ_j^-) are the raising and lowering operators for site j, $\hbar\omega_j$ is the local site excitation energy, $v_{k,l}$ denotes the hopping rate of an excitation between the sites k and l, and Γ_j and γ_j are the dissipative and dephasing rates at site j, respectively. Finally, the transfer efficiency is measured in terms of an irreversible transfer of excitations (with rate $\Gamma_{\text{sink}} = 6.283\ \text{ps}^{-1}$) from site 3 to an extra site 8 modeling the RC, as described by the Lindblad operator

$$\mathcal{L}_{\text{sink}}(\rho) = \Gamma_{\text{sink}} [2\sigma_8^+ \sigma_3^- \rho \sigma_3^+ \sigma_8^- - \{\sigma_3^+ \sigma_8^- \sigma_8^+ \sigma_3^-, \rho\}]. \quad (4)$$

In particular, the transport efficiency is described by the population transferred to the sink $p_{\text{sink}}(t)$, which is given by

$$p_{\text{sink}}(t) = 2\Gamma_{\text{sink}} \int_0^t p_3(t')\, dt', \quad (5)$$

where $p_3(t')$ is the population of site 3 at time t'. Moreover, we choose $\Gamma_j = 5 \times 10^{-4}\ \text{ps}^{-1}$ for any site j, as in Ref. [7]. Notice that decoherence appears in the model above via the action of a pure-dephasing Lindblad superoperator in the master equation for the exciton dynamics, which is equivalent to having stochastic fluctuations of the exciton site energies induced by the environment. This model is known as the Haken-Strobl model and has been used extensively in the chemical physics literature to describe exciton dynamics over several decades [15]. In the next section, we will investigate the entanglement behavior in some non-Markovian models of the FMO complex dynamics with different types of environmental interactions.

Let us stress that, in order to obtain sensible and reliable results for the entanglement analysis, it is crucial that the exciton dynamics be represented by a completely positive map. Indeed, we numerically find that small deviations from the complete positivity conditions are enough to cause significant changes to the entanglement. The Lindblad formalism absolutely guarantees the positivity of the evolving state, whereas the majority of nonperturbative and non-Markovian treatments do not. Hence, in the following, we deem it prudent to choose and to analyze only non-Markovian models that give both reliable entanglement predictions and which are consistent with the essential experimental transport data. Actually, very little is known about the microscopic details of the environment in FMO complex, and it is very hard to distinguish between the various noise models proposed in literature—see for instance Refs. [3,10,16,17]—using the available experimental data. One may conclude that the additional complexity of all of these models results from the introduction of a range of new variables which can be all independently tuned to match the key experimental results, even though the detailed dynamics of these models may be quite different. It should be noted in this respect that the simple Lindbladian model we use here can in fact account for the key features of the experimentally observed dynamics (i.e., long-lived coherence times and transport times)—see Ref. [7].

We will quantify the entanglement across a bipartition $A|B$ of a composite system by using the logarithmic negativity [14], which is

$$E(A|B) = \log_2 ||\rho^{\Gamma_A}||_1, \quad (6)$$

where Γ_A is the partial transpose operation of the density operator ρ with respect to the subsystem A and $||\cdot||_1$ denotes the trace norm. It quantifies how negative the spectrum of the partial transpose of the density matrix is; consequently it is only meaningful if the evolution is completely positive. Furthermore, we would like to stress that in addition to its computational simplicity, the logarithmic negativity also possesses an operational interpretation in terms of the entanglement cost for the exact preparation of the state [18]. When confined to the one excitation subspace, if $A = 1, \ldots, k$ is a set of k chromophores within a global system of N sites, then the logarithmic negativity across the bipartition $(1, \ldots, k)|(k+1, \ldots, N)$ is given by the compact expression

$$E(1, \ldots, k|k+1, \ldots, N) = \log_2 \left(1 - a_{00} + \sqrt{a_{00}^2 + 4X}\right), \quad (7)$$

where $X = \sum_{i=1}^{k} \sum_{j=k+1}^{N} |a_{ij}|^2$, and a_{ij} denotes the off-diagonal element between states with excitations in qubits i and j. Here a_{00} is the matrix element corresponding to the zero-excitation subspace. If all coherences are vanishing (i.e., $a_{ij} = 0$), there is no entanglement across any partition in the one-excitation sector. Note that the restriction to at

most a single excitation is nonproblematic in the case of the logarithmic negativity as it does not affect its definition and the fact that it is an entanglement monotone, that is nonincreasing, for general local operations and classical communication (LOCC). This is not the case if the constraint to at most a single excitation is applied in a way that amends the definition of the functional. In Ref. [19], for example, the global entanglement E_{G}, which is defined as the relative entropy of entanglement with respect to the set $\mathcal{S}$ of totally separable states [20], was amended to yield E_{G1} by replacing the set $\mathcal{S}$ of totally separable states by the set $\mathcal{S}_1$ of totally separable state with at most one excitation. This new function E_{G1} is nonincreasing only when we restrict attention to the set of LOCC operations $\mathcal{O}_1$ that map $\mathcal{S}_1$ onto itself. The set $\mathcal{O}_1$ excludes a wide range of important physical processes such as nondiagonal local unitaries and hence fundamental processes such as laser excitation because the raising operator $a^\dagger \notin \mathcal{O}_1$ does not map $\mathcal{S}_1$ onto itself. Hence, although it is computable, E_{G1} is not an entanglement monotone under natural, physically realizable and important operations that are routinely applied. In fact, the operations permitted in $\mathcal{O}_1$ do not create coherence between the zero and the single excitation sector and hence a more natural interpretation of E_{G1} is one of quantifying coherence rather than entanglement.

Therefore, we will restrict attention to the logarithmic negativity, which is an accepted and at the same time computable entanglement monotone [14] for arbitrary LOCC and arbitrary excitation levels.

III. NON-MARKOVIAN MODELS

To estimate the impact of non-Markovian effects on the entanglement in the FMO complex, we will consider two non-Markovian models of the FMO complex dynamics, each corresponding to a different type of interaction with the surrounding environment. In particular, we assume the FMO complex to be linearly coupled to a bath of damped harmonic oscillators. In all cases, the harmonic oscillators will be damped into a zero temperature bath at rate κ. By using these non-Markovian models, which manifestly preserve the complete positivity of the corresponding quantum evolution, we can study the behavior of the entanglement as measured by the logarithmic negativity and by the entangling power of the quantum evolution itself.

A. Local bath model

While the phenomenon of EET is clearly noise assisted, the exact dynamics within the observed exciton transmission time are strongly model dependent. To further emphasize this aspect and therefore invoke the need for further experimental results, we will present in this section a tunable noise model which reproduces the Markovian results presented in [7] in a certain parameter regime but, interestingly enough, can also provide longer coherence times while preserving and even enhancing EET in a parameter regime where the model exhibits a degree of non-Markovianity. In particular, we consider an environment model motivated by the approach presented by Adolphs and Renger in Ref. [3], where sites interact locally with a quasiresonant localized mode. Their spectral density contains a contribution from a low-energy continuous density of states and a discrete high-energy mode, and its effects on the dynamics of a dimer molecule were recently simulated using a new application of the time-adaptive renormalization group method [21]. Here, for simplicity, we will consider a model in which each FMO chromophore is linearly coupled to a resonant harmonic mode with strength g while each mode is damped into a zero-temperature bosonic reservoir with strength κ. In order to describe these couplings, we add to the previous Hamiltonian in Eq. (1) the following two terms:

$$H_{\mathrm{B}} = \sum_{j=1}^{7} \hbar\omega_h^j a_j^\dagger a_j, \tag{8}$$

$$H_{\mathrm{SB}} = \sum_{j=1}^{7} g_j (a_j + a_j^\dagger)\sigma_j^+ \sigma_j^-, \tag{9}$$

where H_{B} is the free Hamiltonian for the two-level bath with creation and annihilation operators $a^\dagger$ and a, respectively, and mode frequency $\omega_h^j = \omega_j$, and H_{SB} is the system-bath interaction Hamiltonian with interaction strength g. The damping is introduced by considering a Lindblad term $\mathcal{L}_{\mathrm{rad}}^{l-\mathrm{bath}}(\rho)$ of the form

$$\mathcal{L}_{\mathrm{rad}}^{l-\mathrm{bath}}(\rho) = \sum_{j=1}^{7} \kappa_j [-\{a_j^\dagger a_j, \rho\} + 2a_j \rho a_j^\dagger], \tag{10}$$

with k_j being the rate at which the local harmonic mode, coupled to the site j, is damped into a zero-temperature bath. Within the considered parameter regimes, the local modes can be reasonably considered within a two-level approximation. In fact, we numerically monitor the populations in each local mode and find that no local modes are strongly excited or saturated over the whole time interval investigated here. The damping rate κ_i determines the width of the spectrum and hence the correlation time of the local environment associated to site i. For weak coupling and strong mode losses, this approach leads to a Markovian environment with Lorentzian line shape (similar to the models studied by different methods in [21,22]) while, for low losses and strong coupling, the high degree of excitation of the environment leads to deviations from the Lorentzian line shape. To isolate the impact of the non-Markovianity, we keep the ratio g^2/κ (i.e., the effective coupling strength between the site and its mode) fixed while varying the ratio g/κ. To this end, we employ a parameter f to parametrize the system-mode coupling rates $g = \sqrt{f} g_0$ and energy loss rates of the modes with $\kappa = f\kappa_0$. Then, for $f \gg 1$ ($g \ll \kappa$), which is the Markovian limit, we reproduce the optimized dephasing rates found in [7], while for $f \ll 1$ ($g \gg \kappa$) we find non-Markovian behavior. We initiate the system with one excitation in site 1. For a single site, these dynamics were tested to reproduce both the correct Markovian limit and to be capable of exhibiting strongly non-Markovian behavior, as illustrated in Fig. 1. Here, we choose the system-mode coupling rates to be equal to $g_0 = \kappa_0 = \{1,50,41,50,41,5,50\}/5.3$ ps^{-1} to match closely the effective dephasing rates $\{0.157,9.432,7.797,9.432,7.797,0.922,9.433\}$ ps^{-1} in the Markovian limit, as in Ref. [7]. In Fig. 1, we show the entanglement behavior for two different bipartitions of the FMO complex and for two values of f far from the strict Markovian case as well as the time dependence for p_{sink} when

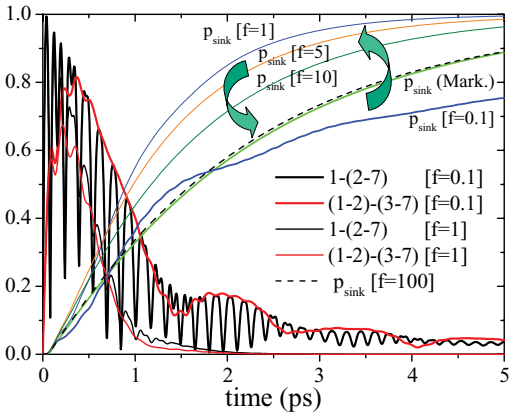

FIG. 1. (Color online) Entanglement of different bi-partitions of the FMO complex dynamics subject to a local form of noise where each FMO site couples to a damped resonant mode. The effective dephasing rates are taken to be equal to the optimal values derived for a fully Markovian model, as in Ref. [7], but the degree of Markovianity of the model can be tuned by varying the parameter f, as described in the text. The entanglement curves are for the 6 splits of the form $(1,\ldots,i)|(i+1,\ldots,7)$, $i \in \{1,\ldots,6\}$, where i corresponds to FMO site i. The behavior of p_{sink} for different values of f is also shown. Large values of f render the dynamics fully Markovian and we recover the results of Ref. [7], whereas one can observe longer coherence times while at the same time enhancing p_{sink} in the low-f domain, as the one exemplified by the value $f = 1$. Note the nonmonotonic behavior of the transfer rate as a function of f, as emphasized by the arrows.

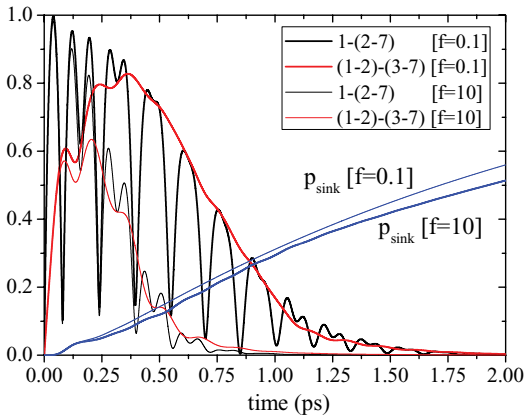

FIG. 2. (Color online) Entanglement of different bipartitions of the FMO complex vs. time (ps), in the presence of a tunable source of noise correlations described by a nonlocal bosonic bath and for different values of the ratio f. For small f, the environmental correlations yield a non-Markovian form of noise and the time scale for entanglement persistence increases while, within this model, the efficiency for transport p_{sink} decreases.

f varies from $f = 0.1$ to 100. The behavior obtained in the fully Markovian case of Ref. [7] is also represented and is indeed already reached for $f = 100$. Interestingly, we obtain that by taking f as our measure of deviation from Markovian behavior, p_{sink} varies nonmonotonically with f so that, in contrast to the nonlocal bath non-Markovian model below or the model described in [22], here the presence of a degree of temporal correlations may even assist the transport of electronic excitations from the antenna to the RC, as seen for values of f in the range 1 to 10. On the other hand, very low values of f (strong non-Markovian case) lead to decreased transport while preserving large values of the coherence across site bipartitions. Note that different noise models, such as the one presented in [23], yield different conclusions. This also shows the great uncertainty about the nature of transport dynamics that arises from our ignorance of the microscopic details of the environment. In this respect, experimental entanglement measurements could be important for removing some of this uncertainty, as it can be very sensitive to the structure of the noise to which the system is subjected [24].

B. Nonlocal bath model

In this subsection, we would like to go further and explore more sophisticated entanglement properties of the entanglement dynamics including its entangling power. Toward this end, we need to further simplify the decoherence model to permit its numerical analysis in the context of the entangling power. This model will also include nonlocal correlations in the environment, and we will start by considering again the entanglement of states in the FMO dynamics under this model and then apply it to the study of the concept of entangling power.

Formally, we consider a model in which we couple each site linearly, with strength g_j, to a single, common harmonic mode damped into a zero-temperature bath at rate κ_j that depends on the location of the excitation [25]. In particular, the following bath-system interaction Hamiltonian term H_{SB} is added to previous Hamiltonian in Eq. (1):

$$H_{\text{SB}} = \sum_{j=1}^{7} g_j (a + a^\dagger)\sigma_j^+ \sigma_j^-, \tag{11}$$

and the damping is described by the following Lindbladian superoperator:

$$\mathcal{L}_{\text{rad}}^{g-\text{bath}}(\rho) = \sum_{j=1}^{7} \kappa_j [-\{\mathbb{P}_j a^\dagger a \mathbb{P}_j, \rho\} + 2\mathbb{P}_j a \rho a^\dagger \mathbb{P}_j], \tag{12}$$

where a and $a^\dagger$ are, respectively, the annihilation and creation operators of the harmonic mode and $\mathbb{P}_j$ is the projector onto site j in the FMO complex. Hence the linewidth of the harmonic oscillator will depend on the location of the excitation. This model mimics closely the model of the previous section in that sites see harmonic oscillators with site-dependent damping rates. At the same time, the Hilbert space of this model is much smaller as the dynamics are restricted to the single excitation sector only. In effect, we can describe the dynamics in the basis $\{|i\rangle|0\rangle, \ldots, |i\rangle|d\rangle\}_{i=1,\ldots,7}$, where the first index refers to the excitation in the FMO complex and the second refers to the environment oscillators. The damping rate of the environment oscillator can be made to depend on the site at which the excitation resides, as would be the case in the local model. Thus, this model represents a mix between the local model in the previous subsection and that of an FMO complex coupled to a single mode; the former allowing for different coupling rates and linewidths for different sites and the latter allowing for a significant reduction in the Hilbert-space dimension of the simulation. In Fig. 2, we consider the entanglement between

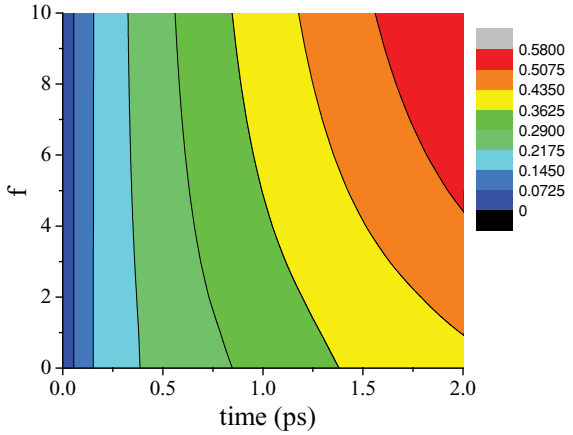

FIG. 3. (Color online) Contour plot for the transfer efficiency in the FMO complex as a function of time (in ps) and of the parameter f for a non-Markovian model with a nonlocal bosonic bath linearly interacting with the FMO.

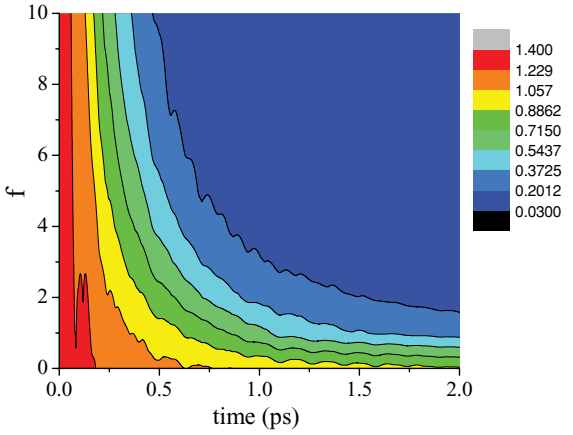

FIG. 4. (Color online) Contour plot for the entangling power in the FMO complex, as a function of time (in ps) and of the parameter f, for the nonlocal-bath non-Markovian model. For low-noise levels, the entangling power of the evolution can be nonmonotonic in time, indicating coherent oscillations in the system. The entangling power decreases monotonically with increasing noise level. In comparison, the entangling power of a CNOT gate is 1, and a SWAP gate is 2. This means that the FMO complex has nontrivial entangling power for a large parameter range.

site 1 and the remainder of the FMO complex as well as sites 1 and 2 versus the remainder of the FMO complex. Here, we choose the system-mode coupling rates as in the local non-Markovian model above, and we find that non-Markovian effects (decreasing f) reduce the transport efficiency while prolonging the lifetime of entanglement. These observations are explained by the fact that the non-Markovian dephasing leads to a reduction of the effective noise level in the system (a phase flip by the environment may be followed by another correlated phase flip at a later time, hence canceling out), upsetting the optimal balance of quantum and incoherent dynamics required for efficient EET [7,8] whilst also increasing and preserving the entanglement that is present in the system. The fact that the presence of a non-Markovian environment may enhance entanglement content beyond the values predicted for an evolution subject to memoryless environments was also predicted when analyzing strictly bipartite systems [26,27], including biological scenarios [28]. Moreover, rather than exploring the entanglement content of states that are generated during the evolution, one may also study quantitatively the entanglement content of the quantum evolution itself. Just as for quantum states, such a quantification is, however, not unique. Here, we consider the capacity of an evolution to create entanglement between two subsystems, each of which may be composed of several components. This automatically provides a lower bound for the amount of entanglement that is required to reproduce the dynamics of the system purely from local operations and classical communication [29,30]. In Figs. 3 and 4, we show a contour plot for the transfer efficiency and the entangling power of the noisy evolution of the FMO complex in the first picoseconds of the EET process, respectively. In particular, we consider the entangling power for the evolution between different bipartitions of the system, quantified by the logarithmic negativity, in the FMO when initially prepared in a maximally entangled state with 7 ancilla qubits. We consider the split $\{\text{qubits } 1_{\text{FMO}}\text{–}1_{\text{ancilla}}\}$–$\{\text{the rest}\}$, as a function of time (in ps) and of the parameter above f. Large quantum correlations are not associated with optimal transport. In the absence of any dephasing, entanglement lasts for times limited only by the excitation loss rate. On the other hand, non-Markovian dephasing (decreasing f) increases the entanglement, which persists for about the initial 20% of the total transmission time, but decreases transport efficiency.

IV. BEYOND SINGLE EXCITONS

So far we have assumed that the system is initialized with a single excitation at site 1. This may not be realized precisely under experimental or natural operating conditions and, furthermore, neglecting higher excitations (though only existing for a really short time) may influence the entanglement content of the system considerably. Hence, a study of quantum entanglement in the FMO complex under realistic conditions should consider a model which allows the freedom to control the number of excitations in the complex at any time. Toward this end, we generalize the theoretical noise model proposed in [6,7] by first modeling (i) the baseplate feeding excitations into the FMO complex as a thermal reservoir of excitations at an effective temperature T and then (ii) a system under laser pulse irradiation.

A. FMO thermal injection

The complex starts in the ground state, without any excitations, which are then introduced into the network via site i with a rate Γ_i. This process is modelled by a thermal bath of harmonic oscillators at a temperature given by the thermal average boson number n_{th}. Within the Markov approximation, the Lindblad superoperator for the injection of excitations takes the form

$$\mathcal{L}_{\text{inj}}(\rho) = n_{\text{th}}\frac{\Gamma_i}{2}[-\{\sigma_i^-\sigma_i^+,\rho\} + 2\sigma_i^+\rho\sigma_i^-] + (n_{\text{th}}+1)\frac{\Gamma_i}{2}[-\{\sigma_i^+\sigma_i^-,\rho\} + 2\sigma_i^-\rho\sigma_i^+], \quad (13)$$

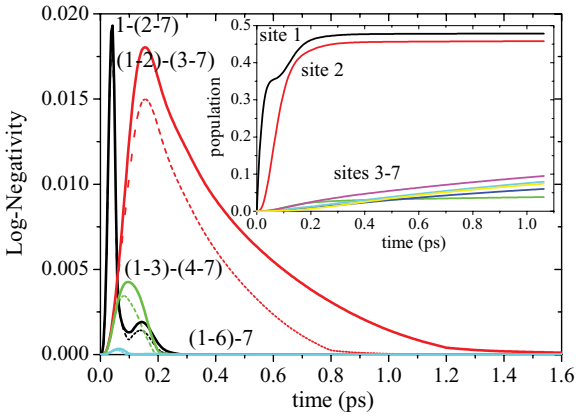

FIG. 5. (Color online) Entanglement, quantified by the logarithmic negativity, in the FMO complex for local (dashed lines) and spatially correlated (continuous lines) dephasing noise, in presence of the thermal injection bath ($n_{\rm th} = 100$, $\Gamma_1 = 1$), within the Markov approximation. The inset shows the site population behavior as a function of time.

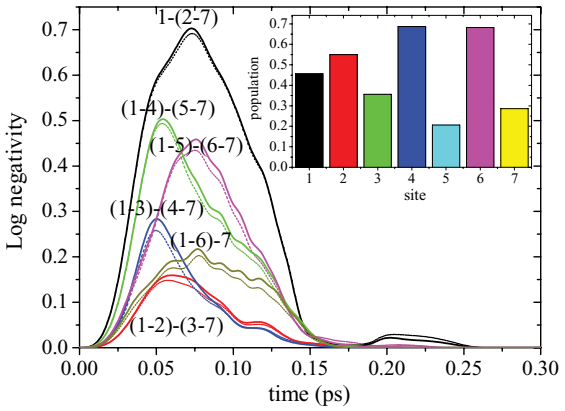

FIG. 6. (Color online) Entanglement in an FMO complex (evolving by a Markovian dynamics) when irradiated with a laser pulse (see the text for more details). Dephasing noise is either local (dashed lines) or spatially correlated (continuous lines). Strong entanglement between sites 1 and 2 is clearly illustrated by the behavior of the top curve [bipartition $1-(2-7)$] as opposed to the bottom one [bipartition $(1-2)-(3-7)$]. Similarly, strong entanglement between sites 5 and 6 is best exemplified by the central plot where we compute the entanglement across bipartition $(1-5)-(6-7)$. The inset shows the site population distribution in the FMO complex for $t = 75$ fs.

which can now be used to study the evolution of quantum entanglement in the FMO complex (or any light-harvesting complex) under various possible natural settings. In particular, motivated by the experimental observations, we choose site 1 as the one at which the excitations are introduced in the FMO complex. In Fig. 5, we show the entanglement time evolution for various subsystems of the qubit network modeling the FMO complex. As can be seen, the amount of entanglement is considerably smaller compared with when the FMO complex starts with exactly one excitation, say on site 1, although it persists on the same timescale [7]. This is because the second term in the injection Liouvillian, which allows for an irreversible loss of excitations from the complex (comparable to spontaneous decay), always accompanies the first one which introduces excitations into the complex. Besides, given the dimensions and structure of the FMO complex (closest site-site distance is $\sim$11 Å), dephasing may not be local, but correlated in space and time [6,7,31,32]. For this reason, we consider also the case of spatially correlated dephasing by using the following Lindblad term:

$$\mathcal{L}^{c}_{\rm deph}(\rho) = -\sum_{m,n} \gamma_{mn}[A_m,[A_n,\rho]], \qquad (14)$$

where γ is a positive semidefinite matrix (to preserve the complete positivity of the quantum evolution), but with the diagonal elements equal to the optimal local dephasing rates as in Ref. [7], and $A_m = \sigma_m^+\sigma_m^-$. Here, the amount and duration of entanglement are both slightly enhanced (solid lines in Fig. 5).

B. FMO laser excitation

In the laboratory [2,4], the complex is typically irradiated with a short laser pulse centered on the typical transition frequencies of the sites. The coupling between the FMO complex and the external radiation field can be described by the semiclassical time-dependent Hamiltonian $H_{\rm FMO-laser}(t)$, which reads in rotating wave approximation as follows:

$$H_{\rm FMO-laser}(t) = -\sum_{i=1}^{7} \vec{\mu}_i \cdot \vec{e}\, E(t)\, e^{-i\omega_1 t}\, \sigma_i^+ + \text{H.c.}, \qquad (15)$$

with $\vec{\mu}_i$ being the molecular transition dipole moment of the individual site i (taken from the published crystal structure in Ref. [33]), $\vec{e}$ being the polarization of the field, and $E(t)$ the time-dependent electric field. In particular, following Ref. [3], we consider a Gaussian electric field pulse of width 60 fs, centered at 120 fs, with an electric field strength $E_0 = 4.97968\ \mathrm{D}^{-1}\cdot\mathrm{cm}^{-1}$, polarized parallel to the dipole moment of site 1 and with a frequency on resonance with the optical transition of site 1 (ω_1). The electric field amplitude was chosen to excite one excitation on site 1 (i.e., to give a π pulse on site 1). However, as the molecular transition dipole moments are of the order of the intersite energy difference, the laser pulse leads to excitation of all sites. We have studied this scenario as well, both for local and correlated spatial dephasing noise, and the results are presented in Fig. 6. This scenario generates a considerable amount of entanglement (although for a shorter amount of time compared with the previous scenario), and it might be concluded that, although an FMO complex operating in nature may not possess substantial amounts of entanglement, it is possible in the laboratory to generate large amounts of it. This could open up new vistas for exploring quantum effects in biological systems, albeit under laboratory conditions, and also allow for a demonstration of entanglement enhancement for the non-Markovian case.

V. MODE ENTANGLEMENT

When local addressing is unfeasible, site entanglement is directly immeasurable, even when the evolution is confined

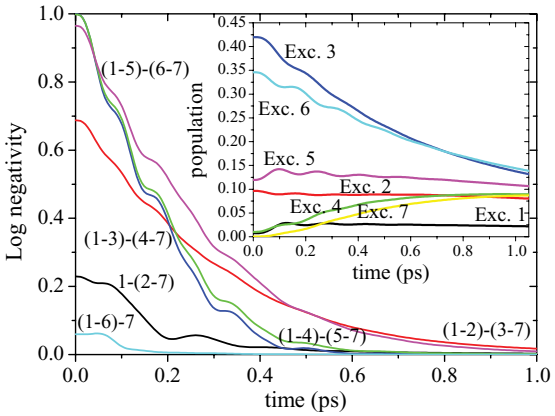

FIG. 7. (Color online) The logarithmic negativity in the FMO complex (evolving by Markovian dynamics) for local dephasing noise in the exciton basis. Initially, one excitation is in site 1. The curves are for the 6 splits of the form $(1,\ldots,i)|(i+1,\ldots,7), i \in \{1,\ldots,6\}$, where now i corresponds to exciton i and they are ordered with increasing exciton energies. Inset shows exciton population vs. time (ps).

to the single-excitation sector. However, the evaluation of mode entanglement via the experimental determination of coherences in the exciton basis can provide information about the existence of quantum correlations in the system. The temporal behavior of mode entanglement within our Markovian model [7] and for different bipartitions is shown in Fig. 7, together with the exciton populations along the first ps of the EET. Initially all modes are populated, with the largest fraction in excitons 3 and 6, which leads to high values of mode entanglement across bipartitions, each containing one of those high-energy excitons. As time elapses, entanglement degrades monotonically as the transfer efficiency increases.

VI. CONCLUSIONS AND OUTLOOK

Efficient EET in light-harvesting complexes can be traced back to an interplay between coherent and incoherent processes where the quantum correlations characteristic of the coherent evolution are partially suppressed by noise, yet not entirely destroyed. We have placed the analysis of entanglement in such systems on a quantitative footing and have shown that for optimal transport the entanglement, while present, is neither maximal nor long lived. Actually, long-lived entanglement exists in the absence of dephasing, which is known to be highly inefficient. However, despite the fact that observed transfer times do require noise-assisted transport dynamics, it turns out that the time dependence of both coherences and population transfer over the full transfer time are strongly model dependent.

In summary, an interplay between creation of entanglement for short distances and times (through coherent interaction) followed by the destruction of entanglement for longer distance and times (through dephasing noise) seems to be necessary for optimal transport. Moreover, our entanglement results could actually be seen as providing a potential experimental test for the form of the system-environment coupling. Unlike the coherence and transport times, the entanglement is sensitive to the precise evolution of the system, and an experiment that could measure entanglement (such experiments are indeed planned), could differentiate between models. In order to do so, the entanglement predictions for various noise models must be available for comparison, and in this respect the nature of the environment is central to the problem of energy transport in photosynthetic complexes. Further studies are, however, required before any result can be accepted as conclusive on the functional and possibly beneficial role of coherence and entanglement in EET.

ACKNOWLEDGMENTS

A.W.C. is most grateful to G.R. Fleming and his group for their hospitality. This work was supported by the EPSRC, the EU projects QAP and CORNER, and the Humboldt Foundation. F.C. was also supported by a Marie Curie Intra European Fellowship within the 7th European Community Framework Programme.

[1] T. Förster, Ann. Phys. (Leipzig) **2**, 55 (1948); A. G. Redfield, Adv. Magn. Reson. **1**, 1 (1965); M. Grover and R. Silbey, J. Chem. Phys. **54**, 4843 (1971); G. D. Scholes, Annu. Rev. Phys. Chem. **54**, 57 (2003).

[2] H. Lee, Y.-C. Cheng, and G. R. Fleming, Science **316**, 1462 (2007); V. I. Prokhorenko *et al.*, J. Phys. Chem. B **106**, 9923 (2002).

[3] J. Adolphs and T. Renger, Biophys. J. **91**, 2778 (2006).

[4] G. S. Engel, T. R. Calhoun, E. L. Read, T.-K. Ahn, T. Manal, Y.-C. Cheng, R. E. Blankenship, and G. R. Fleming, Nature (London) **446**, 782 (2007).

[5] M. Mohseni, P. Rebentrost, S. Lloyd, and A. Aspuru-Guzik, J. Chem. Phys. **129**, 174106 (2008).

[6] M. B. Plenio and S. F. Huelga, New J. Phys. **10**, 113019 (2008).

[7] F. Caruso, A. W. Chin, A. Datta, S. F. Huelga, and M. B. Plenio, J. Chem. Phys. **131**, 105106 (2009).

[8] A. W. Chin, A. Datta, F. Caruso, S. F. Huelga, and M. B. Plenio, New J. Phys. **12**, 065002 (2010).

[9] A. Olaya-Castro, C. F. Lee, F. F. Olsen, and N. F. Johnson, Phys. Rev. B **78**, 085115 (2008).

[10] A. Ishizaki and G. R. Fleming, Proc. Natl. Acad. Sci. **106**, 17255 (2009).

[11] S. Hoyer, M. Sarovar, and K. B. Whaley, e-print arXiv:0910.1847 (2009).

[12] F. Caruso, S. F. Huelga, and M. B. Plenio, e-print arXiv:1003.5877.

[13] M. B. Plenio, Phys. Rev. Lett. **95**, 090503 (2005); J. Eisert, Ph.D. thesis, University of Potsdam (2001); J. Eisert and M. B. Plenio, J. Mod. Opt. **46**, 145 (1999).

[14] M. B. Plenio and S. Virmani, Quant. Inf. Comp. **7**, 1 (2007).
[15] H. Haken and G. Strobl, Z. Phys. **262**, 135 (1973); V. M. Kenkre and P. Reineker, *Exciton Dynamics in Molecular Crystals and Aggregates* (Springer-Verlag, Berlin, 1982).
[16] L. Z. Sharp, D. Egorova, and W. Domcke, J. Chem. Phys. **132**, 014501 (2010).
[17] M. Sarovar, Y.-C. Cheng, and K. B. Whaley, e-print arXiv:0911.5427.
[18] K. M. R. Audenaert, M. B. Plenio, and J. Eisert, Phys. Rev. Lett. **90**, 027901 (2003).
[19] M. Sarovar, A. Ishizaki, G. R. Fleming, and K. B. Whaley, Nat. Phys. **6**, 462 (2010).
[20] V. Vedral and M. B. Plenio, Phys. Rev. A **57**, 1619 (1998).
[21] J. Prior, A. W. Chin, S. F. Huelga, and M. B. Plenio, e-print arXiv:1003.5503.
[22] A. Ishizaki and G. R. Fleming, J. Chem. Phys. **130**, 234110 (2009).
[23] P. Rebentrost, R. Chakraborty, and A. Aspuru-Guzik, J. Chem. Phys. **131**, 184102 (2009).
[24] A. G. Dijkstra and Y. Tanimura, e-print arXiv:1004.1450.
[25] A finite temperature setting may also be implemented by initializing the mode in a thermal state at temperature T and coupling the mode to a Markovian environment at temperature T.
[26] B. Bellomo, R. Lo Franco, and G. Compagno, Phys. Rev. Lett. **99**, 160502 (2007).
[27] I. Sinayskiy, E. Ferraro, A. Napoli, A. Messina, and F. Petruccione, J. Phys. A **42**, 485301 (2009).
[28] M. Thorwart, J. Eckel, J. H. Reina, P. Nalbacha, and S. Weiss, Chem. Phys. Lett. **478**, 234 (2009).
[29] J. Eisert, K. Jacobs, P. Papadopoulos, and M. B. Plenio, Phys. Rev. A **62**, 052317 (2000).
[30] P. Zanardi, C. Zalka, and L. Faoro, Phys. Rev. A **62**, 030301(R) (2000).
[31] E. Hennebicq, D. Beljonne, C. Curutchet, G. D. Scholes, and R. J. Silbey, J. Chem. Phys. **130**, 214505 (2009).
[32] F. Fassioli, A. Nazir, and A. Olaya-Castro, e-print arXiv:0907.5183.
[33] D. E. Tronrud, M. F. Smidt, and B. E. Mattthews, J. Mol. Biol. **188**, 443 (1986).